

# Magnetization process of the spin-1/2 $XXZ$ models on square and cubic lattices

Masanori Kohno and Minoru Takahashi

*Institute for Solid State Physics,*

*University of Tokyo, Roppongi, Minato-ku, Tokyo 106*

(October 6, 2018)

## Abstract

The magnetization process of the spin-1/2 antiferromagnetic  $XXZ$  model with Ising-like anisotropy in the ground state is investigated. We show numerically that the Ising-like  $XXZ$  models on square and cubic lattices show a first-order phase transition at some critical magnetic field. We estimate the value of the critical field and the magnetization jump on the basis of the Maxwell construction. The magnetization jump in the Ising-limit is investigated by means of perturbation theory. Based on our numerical results, we briefly discuss the phase diagram of the extended Bose-Hubbard model in the hard-core limit.

PACS numbers: 75.30.Kz, 75.40.Cx, 05.30.Jp, 67.40.Db

## I. INTRODUCTION

Néel [1] predicted the first-order transition of anisotropic antiferromagnets in the presence of a magnetic field in 1936. He pointed out that the spins will abruptly change directions from parallel to perpendicular with respect to the  $c$ -axis (easy axis of sublattice magnetization) at some value of the external magnetic field, when the magnetic field is applied to the direction parallel to the  $c$ -axis. His prediction was confirmed experimentally [2], and this first-order phase transition is now known as the spin-flopping process. Thirty years later than the discovery of the spin-flopping process, C.N. Yang and C.P. Yang showed by the Bethe ansatz that the one-dimensional (1d) spin-1/2  $XXZ$  model with Ising-like anisotropy exhibits a second-order transition in the presence of a magnetic field [3]. Thus, for one-dimensional Ising-like antiferromagnets, quantum fluctuations, which are neglected in the mean-field approximation, play an essential role. In this way, quantum fluctuations may drastically modify the classical behavior depending on the dimensionality. Hence, we investigate the magnetization process of the spin-1/2 Ising-like  $XXZ$  (I- $XXZ$ ) models in two and three dimensions in order to see how quantum fluctuations modify the classical behavior of the magnetization process of Ising-like antiferromagnets.

Also, the spin-1/2  $XXZ$  model can be translated into the hard-core boson model with nearest neighbor repulsion [4]. This model corresponds to a special case of the extended Bose-Hubbard model which is considered to be relevant for low-temperature properties of liquid helium on a periodic substrate and also for Josephson junction arrays [5–7]. From the theoretical point of view, a lot of attention has been paid to the Bose-Hubbard model as the simplest model to describe the superfluid-insulator transition [5–9]. We can obtain information about the superfluid-insulator transition occurring in the extended Bose-Hubbard model through the investigation of the spin-1/2 I- $XXZ$  model.

This paper is organized as follows: In Sec. II, the  $XXZ$  model is defined. The details of the numerical calculations are presented. In Sec. III, we review the classical Ising-like  $XXZ$  model. Numerical results on the magnetization curve of the spin-1/2 I- $XXZ$  models in two

and three dimensions are shown in Sec. IV. In Sec. V, the behavior of the magnetization curve in the Ising-limit is investigated by means of perturbation theory. In Sec. VI, we briefly discuss the superfluid-insulator transition in the extended Bose-Hubbard model in the hard-core limit based on the numerical results of the spin-1/2 I- $XXZ$  model. Section VII is devoted to summary.

## II. MODEL AND METHOD

In the present paper, we consider the  $XXZ$  model defined by the following Hamiltonian:

$$\mathcal{H}_{XXZ} = J \sum_{\langle i,j \rangle} (S_i^x S_j^x + S_i^y S_j^y + \lambda S_i^z S_j^z), \quad (2.1)$$

where  $S_i^{x(y,z)}$  denote the  $x(y,z)$  components of the spin operator at site  $i$ . Here  $\langle i,j \rangle$  denotes nearest neighbors. The anisotropic coupling constant is denoted by  $\lambda$ . For  $\lambda = 1$ , the isotropic Heisenberg model is recovered. We investigate the spin-1/2  $XXZ$  models on square and cubic lattices in the ground state in the canonical ensemble. Namely, we measure the energy  $E$  within the subspace of fixed magnetization  $M$  ( $=\sum_i S_i^z$ ). The magnetic field in a finite-size cluster is defined as  $H(\bar{M}) \equiv (E(M_1) - E(M_2))/(M_1 - M_2)$ , where  $\bar{M}$  is defined by  $(M_1 + M_2)/2$ . In the thermodynamic limit, this definition of the magnetic field reduces to the normal one:  $H \equiv \partial E / \partial M$ . The maximum magnetization and the saturation field are denoted by  $M_{\max}(=N_s/2)$  and  $H_{\max}(=J(\lambda + 1)d)$ , respectively. Here  $N_s$  and  $d$  are the system size and the spatial dimensionality.

We use the Lanczos algorithm (exact diagonalization) for clusters up to 32 sites and the cluster algorithm [10] (quantum Monte Carlo) for larger clusters up to 100 sites. For the cluster algorithm, the measurements have been performed at the inverse temperature  $\beta J = 16$ . The width of the Trotter slice is chosen as  $\Delta\tau J = 0.04$  for two dimensions (2d) and  $\Delta\tau J = 0.053$  for three dimensions (3d). The simulation has been performed in the canonical ensemble. In the small  $\lambda$  regime, the number of points near  $M = 0$  obtained by exact diagonalization is too small to use the Maxwell construction. On the other hand, in

the large  $\lambda$  regime, statistical errors in the quantum Monte Carlo calculation become large, because the spin configurations are almost frozen. Hence, we have investigated the small  $\lambda$  regime by quantum Monte Carlo and the large  $\lambda$  regime by exact diagonalization.

In order to see finite-size effects, we show the size-dependence of the energy gap  $\Delta_g (\equiv E(M=1) - E(M=0))$ , the critical field  $H_c$  and the magnetization jump  $M_s$  in Fig.1. As shown in this figure, the size-dependence is very small. As a check of numerical accuracy, we compare the energy gap  $\Delta_g$  obtained by this method with those obtained by other methods as shown in Fig.2. Our result is quite consistent with those of third-order spin-wave theory [11] and the series expansion around the Ising-limit [12]. Hence, we consider that the inverse temperature  $\beta$  and the width of the Trotter slice  $\Delta\tau$  are sufficient. [See also Fig.4.] For three dimensions, we report the 64-site results.

### III. REVIEW OF THE CLASSICAL SPIN CASE

Before investigating the spin-1/2  $XXZ$  models, we briefly review the magnetization process of the classical I- $XXZ$  model in the ground state [1,13]. The ground state energy of the classical I- $XXZ$  model may be written in the following form:

$$\begin{aligned} E_{C-XXZ} &= \frac{JN_s z}{2} (S_A^x S_B^x + S_A^y S_B^y + \lambda S_A^z S_B^z) \\ &= -\frac{JN_s z S^2}{2} (\sin(\theta + \phi) \sin(\theta - \phi) \\ &\quad + \lambda \cos(\theta + \phi) \cos(\theta - \phi)), \end{aligned} \quad (3.1)$$

where  $S_{A(B)}^{x(y,z)}$  represent the  $x(y,z)$  components of the spin operators at a site in the A(B) sublattices. The length of the spin and the coordination number are denoted by  $S$  and  $z(=2d)$ , respectively. The angles  $\theta$  and  $\phi$  are defined as in Fig.3(a) ( $0 \leq \theta \leq \pi/2$ ,  $0 \leq \phi \leq \pi/2$ ).

The Zeeman term  $E_Z$  is written in the following form:

$$E_Z = -\frac{HN_s}{2} (S_A^z + S_B^z) = \frac{HN_s S}{2} (\cos(\theta + \phi) - \cos(\theta - \phi)). \quad (3.2)$$

By minimizing the total energy ( $E_{\text{tot}} \equiv E_{C-XXZ} + E_Z$ ) with respect to  $\theta$  and  $\phi$ , one finds the following stable states (Fig.3(b)):

- (i)  $\theta = 0, \quad \phi = 0, \quad E_{\text{tot}} = -\tilde{J}\lambda \quad \text{for } \tilde{H} < \tilde{J}\sqrt{\lambda^2 - 1}$
- (ii)  $\theta = \pi/2, \phi = \arcsin \frac{\tilde{H}}{\tilde{J}(\lambda+1)}, E_{\text{tot}} = -\tilde{J} - \frac{\tilde{H}^2}{\tilde{J}(\lambda+1)} \text{ for } \tilde{J}(\lambda+1) > \tilde{H} > \tilde{J}\sqrt{\lambda^2 - 1}$
- (iii)  $\theta = \pi/2, \phi = \pi/2, \quad E_{\text{tot}} = \tilde{J}\lambda - 2\tilde{H} \quad \text{for } \tilde{H} > \tilde{J}(\lambda+1),$

where  $\tilde{J}$  and  $\tilde{H}$  are defined as  $\tilde{J} \equiv JN_s z S^2/2$  and  $\tilde{H} \equiv HN_s S/2$ . The magnetization curve of the classical I-XXZ model is shown in Fig.3(c). The transition from the state (i) to the state (ii) is known as the spin-flopping process [1,13]. The critical field  $H_c$  is defined as the magnetic field above which the ground state has non-zero magnetization. The  $\lambda$  dependence of the critical field  $H_c$  and that of the magnetization jump  $M_s$  are obtained as

$$H_c/H_{\text{max}} = M_s/M_{\text{max}} = \sqrt{(\lambda - 1)/(\lambda + 1)}, \quad (3.3)$$

where  $H_{\text{max}} = JSz(\lambda + 1)$  and  $M_{\text{max}} = N_s S$ .

#### IV. MAGNETIZATION CURVE OF THE SPIN-1/2 XXZ MODEL

In this section, we present the numerical results on the magnetization curve of the spin-1/2 I-XXZ models on square and cubic lattices. As an example, we show the magnetization curve of the spin-1/2 XXZ model for  $\lambda = 2$  on a square lattice in Fig. 4. The critical field  $H_c$  and the magnetization jump  $M_s$  are determined on the basis of the Maxwell construction as follows. [See also Fig.9(a).] We fit the energy as a function of magnetization by a polynomial. The tangent from the point at  $M = 0$  to the fitting curve gives a lower energy than the numerical data in the region of  $0 < M < M_s$ . Here  $M_s$  is the magnetization at the point of contact between the fitting curve and the tangent. Hence, we can identify the region of phase separation as  $0 < M < M_s$  on the basis of the Maxwell construction [14]. The magnetic field of the phase-separated state ( $H_c$ ) is given as the slope of the tangent. In practice, we have determined the phase-separation boundary as the point where the following condition is satisfied:  $\partial E/\partial M = (E(M) - E(M = 0))/M$  as in Fig.5. The size-dependence of the critical field  $H_c$  and that of the magnetization jump  $M_s$  determined by the Maxwell construction are very small as discussed in Sec.II (Fig.1).

We show the  $\lambda$  dependence of the critical field  $H_c$  in Fig.6. The critical field  $H_c$  is suppressed by quantum fluctuations. In order to see how large the critical field  $H_c$  is suppressed by quantum fluctuations, we have tried to fit the numerical data as  $H_c/H_{\max} = (\frac{\lambda-1}{\lambda+1})^\alpha$ , analogously with the classical result  $\alpha = 0.5$  (eq.(3.3)). We estimate  $\alpha$  to be  $\alpha = 0.64 \pm 0.01$  for 2d and  $\alpha = 0.57 \pm 0.01$  for 3d. Note that the  $\lambda$  dependence of the critical field  $H_c$  in two and three dimensions is quite different from the one-dimensional case, where the gap ( $=H_c \equiv \partial E/\partial M|_{M/M_{\max} \rightarrow +0}$ ) opens exponentially:  $H_c \propto \exp[-\pi^2/2\sqrt{2(\lambda-1)}]$  [15].

Here, we mention the relation between the critical field  $H_c$  and the energy gap  $\Delta_g$ . It is expected that the energy gap  $\Delta_g$  is larger than the critical field  $H_c$ , if a first-order transition occurs in the presence of a magnetic field. The reason is as follows. The ground state of  $M = 1$  is considered to be the one-magnon state, which may be described by spin-wave theory. Hence, the gap  $\Delta_g$  corresponds to the excitation energy of one magnon from the ground state of  $M = 0$ . On the other hand, phase separation occurs, because magnons gain energy by interacting attractively with each other. The critical field  $H_c$  would be determined by the effective attractive interactions between the macroscopic number of magnons. As a result, if phase separation occurs, the gap  $\Delta_g$  is expected to be larger than the critical field  $H_c$ , i.e.

$$\Delta_g > H_c \equiv \partial E/\partial M|_{M/M_{\max} \rightarrow +0}, \quad (4.1)$$

where  $M$  is assumed to be a macroscopic number when the limit  $M/M_{\max} \rightarrow +0$  is taken. We compare the gap  $\Delta_g$  and the critical field  $H_c$  of the spin-1/2 I-XXZ model on a square lattice in Fig.7. The gap  $\Delta_g$  is always larger than the critical field  $H_c$  as expected. It is interesting to contrast this behavior with the one-dimensional result. For one dimension, the transition is of second order [3], and the following relation is satisfied:  $\partial E/\partial M|_{M/M_{\max} \rightarrow +0} = E(M=1) - E(M=0)$ . This is considered to be due to effective repulsive interactions.

The  $\lambda$  dependence of the magnetization jump  $M_s$  is shown in Fig.8. We estimate the critical value of  $\lambda$ , where  $M_s$  vanishes, as  $\lambda_c = 1.00 \pm 0.02$  by extrapolating the data in Fig.8. This confirms that the spin-1/2 I-XXZ models on square and cubic lattices show a

first-order transition at some critical field for any value of the anisotropic coupling constant larger than one ( $\lambda > 1$ ). The  $\lambda$  dependence of the magnetization jump  $M_s$  is remarkably different from the classical result, especially in the large  $\lambda$  regime.

## V. ISING-LIMIT

In this section, we discuss the magnetization process of the spin-1/2  $XXZ$  model in the Ising-limit. In Fig.8, the value of the magnetization jump  $M_s$  in the Ising-limit ( $\lambda \rightarrow \infty$ ) does not coincide with that of the Ising model ( $\lambda = \infty$ ) ( $M_s(\lambda = \infty) = M_{\max}$ ):

$$M_s(\lambda \rightarrow \infty) \neq M_s(\lambda = \infty). \quad (5.1)$$

This can be explained by means of perturbation theory as follows. We rewrite the spin-1/2  $XXZ$  model as

$$\mathcal{H}_{XXZ} = \bar{J} \sum_{\langle i,j \rangle} S_i^z S_j^z + \epsilon \bar{J} \sum_{\langle i,j \rangle} (S_i^x S_j^x + S_i^y S_j^y), \quad (5.2)$$

where  $\bar{J}$  and  $\epsilon$  are defined as  $\bar{J} \equiv J\lambda$  and  $\epsilon \equiv 1/\lambda$ . We consider the  $XY$ -term as the perturbation. At  $M = 0$ , the unperturbed ground states are the two-degenerate Néel states. The leading perturbation energy is of order  $\epsilon^2$ . On the other hand, in the limit of  $M \rightarrow M_{\max}$ , the leading perturbation energy is of order  $\epsilon$  and proportional to  $M - M_{\max}$ . Hence it is expected that phase separation occurs for the magnetization smaller than some value  $M_s(< M_{\max})$  in the Ising-limit. We numerically estimate the value of  $M_s$  in the Ising-limit with first-order perturbation theory in the following way. The first-order perturbation energy  $E_1$  is obtained as

$$E_1 = \frac{\epsilon \bar{J} \sum_{\alpha, \beta} \langle \beta | \sum_{\langle i,j \rangle} (S_i^+ S_j^- + S_i^- S_j^+) | \alpha \rangle}{2 \sum_{\alpha} \langle \alpha | \alpha \rangle}, \quad (5.3)$$

where  $|\alpha\rangle$  and  $|\beta\rangle$  denote unperturbed ground states of the Ising model in the subspace of fixed magnetization. We generate  $|\alpha\rangle$ 's randomly and measure  $E_1$  using Monte Carlo technique. The value of  $M_s$  is determined based on the Maxwell construction. Figure 9

shows the first-order perturbation energy  $E_1$  and the value of  $M_s$  in the Ising-limit on hyper-cubic lattices in dimensions up to six. We extrapolate the data in Fig.9(b) and estimate the inverse dimensionality, where  $M_s$  coincides with  $M_{\max}$ , as  $1/d = 0.01 \pm 0.02$ . This confirms that the value of  $M_s$  in the Ising-limit ( $\lambda \rightarrow \infty$ ) does not coincide with that of the Ising model ( $\lambda = \infty$ ) in finite spatial dimensions.

## VI. RELATION TO THE BOSE-HUBBARD MODEL

In this section, we briefly discuss the phase diagram of the hard-core boson model with nearest-neighbor repulsion based on the numerical results of the spin-1/2  $XXZ$  models. The hard-core boson model with nearest-neighbor repulsion can be obtained from the following extended Bose-Hubbard model by taking the on-site repulsion  $U$  infinity:

$$\mathcal{H}_{\text{BH}} = t \sum_{\langle i,j \rangle} (b_i^\dagger b_j + b_j^\dagger b_i) + U \sum_i n_i(n_i - 1) + V \sum_{\langle i,j \rangle} (n_i - 1/2)(n_j - 1/2), \quad (6.1)$$

where  $b_i^\dagger$  ( $b_i$ ) creates (annihilates) a boson on site  $i$  and  $n_i = b_i^\dagger b_i$ . Here  $\langle i, j \rangle$  denotes nearest neighbors. The spin-1/2  $XXZ$  model can be translated into the hard-core boson model with nearest-neighbor repulsion ( $t \leftrightarrow J/2$ ,  $V \leftrightarrow J\lambda/4$ ) [4]. Figure 8 corresponds to the phase diagram of this model by relating the filling  $\rho$  and the interaction strength  $V/t$  to  $M/M_{\max}$  and  $\lambda$  according to  $\rho = (1 - M/M_{\max})/2$  and  $V/t = \lambda/2$ . The numerical results in the previous section are translated as follows: The superfluid-insulator transition occurs in the region of  $V > t/2$ . This transition is a first-order transition, which is consistent with recent investigation of the Bose-Hubbard model [9]. Phase separation does not occur for the density  $\rho$  smaller than  $\rho_c$ , for finite  $V/t$ , where  $\rho_c \equiv (1 - M_s(\lambda \rightarrow \infty)/M_{\max})/2 > 0$ . This  $\rho_c$  approaches zero as the spatial dimensionality  $d$  goes to infinity (Fig.9(b)).

## VII. SUMMARY

In summary, numerical results on the magnetization process of the spin-1/2 Ising-like  $XXZ$  models have been reported. The spin-1/2  $XXZ$  models on square and cubic lattices



show a first-order phase transition at some critical magnetic field for the anisotropic coupling constant larger than one ( $\lambda > 1$ ). The critical field  $H_c$  and the magnetization jump  $M_s$  are estimated on the basis of the Maxwell construction. The critical field  $H_c$  is suppressed by quantum fluctuations (Fig.6). We have demonstrated that the energy gap  $\Delta_g$  is larger than the critical field  $H_c$  (Fig.7). The anisotropy  $\lambda$  dependence of the magnetization jump  $M_s$  is remarkably different from the classical result (Fig.8). It is strongly suggested that the value of  $M_s$  in the Ising-limit ( $\lambda \rightarrow \infty$ ) does not coincide with that of the Ising model ( $\lambda = \infty$ ) in finite spatial dimensions due to quantum effects (Fig.9).

### ACKNOWLEDGMENTS

The authors would like to thank H.Shiba for helpful discussions and useful comments. One of the authors (M.K.) thanks T. Kawarabayashi, E. Williams and D. Lidsky for reading of the manuscript. The exact diagonalization program is based on the subroutine package "TITPACK Ver.2" coded by H. Nishimori. Part of the calculations were performed on the Fujitsu VPP500 and on the Intel Japan PARAGON at Institute for Solid State Physics, Univ. of Tokyo.

## REFERENCES

- [1] L. Néel, *Ann. de Phys.* **5**, 232 (1936).
- [2] N.J. Poulis, J. van den Handel, J. Ubbink, J.A. Poulis and C.J. Gorter, *Phys. Rev.* **82**, 552 (1951).
- [3] C.N. Yang and C.P. Yang, *Phys. Rev.* **151**, 258 (1966).
- [4] T. Matsubara and H. Matsuda, *Prog. Theor. Phys.* **16**, 569 (1956); **17**, 19 (1957).
- [5] M.P.A. Fisher, P.B. Weichman, G. Grinstein and D.S. Fisher, *Phys. Rev. B* **40**, 546 (1989).
- [6] M.-C. Cha, M.P.A. Fisher, S.M. Girvin, M. Wallin and A.P. Young, *Phys. Rev. B* **44**, 6883 (1991).
- [7] C. Bruder, R. Fazio, A. Kampf, A. van Otterlo and G. Schön, *Phys. Scr.* **42**, 159 (1992); C. Bruder, R. Fazio and G. Schön, *Phys. Rev. B* **47**, 342 (1993).
- [8] A. van Otterlo and K.-H. Wagenblast, *Phys. Rev. Lett.* **72**, 3598 (1994); A. van Otterlo, *Phys. Rev. B* **52**, 16176 (1995).
- [9] R.T. Scalettar, G.G. Batrouni, A.P. Kampf and G.T. Zimanyi, *Phys. Rev. B* **51**, 8467 (1995); G.G. Batrouni, R.T. Scalettar, G.T. Zimanyi and A.P. Kampf, *Phys. Rev. Lett.* **74**, 2527 (1995).
- [10] H.G. Evertz, G. Lana and M. Marcu, *Phys. Rev. Lett.* **70**, 875 (1993); N. Kawashima and J.E. Gubernatis, *Phys. Rev. E* **51**, 1547 (1995).
- [11] C.J. Hamer, Z. Weihong and P. Arndt, *Phys. Rev. B* **46**, 6276 (1992).
- [12] Z. Weihong, J. Oitmaa, and C.J. Hamer, *Phys. Rev. B* **43**, 8321 (1991).
- [13] K. Yosida, *Prog. Theor. Phys.* **6**, 691 (1951).
- [14] The finite-size effects on the energy in the phase-separated state may be much larger

than those in a homogeneous state because of macroscopic fluctuations. The system sizes examined in this paper may be insufficient to obtain an accurate value for the energy of the phase-separated state. Therefore we use the Maxwell construction to determine it.

- [15] J.D. Cloizeaux and M. Gaudin, J. Math. Phys. **7**, 1384 (1966).

## FIGURES

FIG. 1. Size dependence of the critical field  $H_c$  [(a)], the magnetization jump  $M_s$  [(b)] and the energy gap [(c)]  $\Delta_g$  on the two-dimensional spin-1/2  $XXZ$  model. Dotted lines are guides to the eye.

FIG. 2. Energy gap  $\Delta_g$  for the two-dimensional spin-1/2  $XXZ$  model. Open circles and open squares denote the results obtained by third-order spin-wave theory cited from [11] and the series expansion cited from [12], respectively. Solid and dotted lines correspond to the classical and one-dimensional cases, respectively.

FIG. 3. (a) Definition of  $\theta$  and  $\phi$ . (b) Schematic picture of stable spin-configurations. (i) Néel state. (ii) spin flopping state. (iii) fully polarized state. (c) Magnetization curve of the classical  $XXZ$  model with Ising-like anisotropy.

FIG. 4. Magnetization curve of the two-dimensional spin-1/2  $XXZ$  model with Ising-like anisotropy. Open and solid symbols denote the data in 26-site and 36-site clusters, respectively. Solid (dotted) lines correspond to the phase-separated states determined on the basis of the Maxwell construction by using the data in 36-site (26-site) clusters. We choose  $M_1 - M_2 = 1$  or 2 in the definition of the magnetic field  $H$ . The definition of the magnetic field  $H$  is in the text. The 36-site data for  $0 < M/M_{\max} < 0.6$  are obtained by quantum Monte Carlo. Other data are obtained by exact diagonalization.

FIG. 5.  $\partial E/\partial M$  (solid symbols) and  $(E(M) - E(M = 0))/M$  (open symbols). The intersection point of two curves corresponds to the phase-separation boundary. The data are obtained by exact diagonalization in a 26-site cluster ( $\lambda = 2$ ). We set  $J = 1$ .

FIG. 6. Anisotropy  $\lambda$  dependence of the critical field  $H_c$  of the spin-1/2  $XXZ$  model. (a) Linear plot and (b) Log-log plot. Solid and dotted lines correspond to the classical and one-dimensional cases, respectively. Dashed and dash-dotted lines correspond to the cases  $\alpha = 0.64$  and  $\alpha = 0.57$ . The definition of  $\alpha$  is in the text.

FIG. 7. Anisotropy  $\lambda$  dependence of the energy gap  $\Delta_g$  (solid symbols) and the critical field  $H_c$  (open symbols) of the spin-1/2  $XXZ$  model on a square lattice. Solid and dotted lines correspond to the classical and one-dimensional cases, respectively.

FIG. 8. Anisotropy  $\lambda$  dependence of the magnetization jump  $M_s$  of the spin-1/2  $XXZ$  model. The solid line corresponds to the classical case. Bold lines are guides to the eye. This figure corresponds to the phase diagram of the hard-core boson model with nearest-neighbor repulsion by relating the filling  $\rho$  and the interaction strength  $V/t$  to  $M/M_{\max}$  and  $\lambda$  according to  $\rho = (1 - M/M_{\max})/2$  and  $V/t = \lambda/2$ . The definition of the hard-core boson model is in the text.

FIG. 9. (a) First-order perturbation energy in the Ising-limit on hyper-cubic lattices. We set  $J = 1$  as the energy unit. The system sizes are 400 sites for 2d, 1000 sites for 3d, 1296 sites for 4d, 1024 sites for 5d and 4096 sites for 6d. Dashed lines denote the tangents from  $M = 0$ . The magnetization at the point of contact corresponds to  $M_s$ . (b) Dimensionality  $d$  dependence of  $M_s$  in the Ising-limit on hyper-cubic lattices. The dashed line represents  $M_s/M_{\max} = 1/d$ .

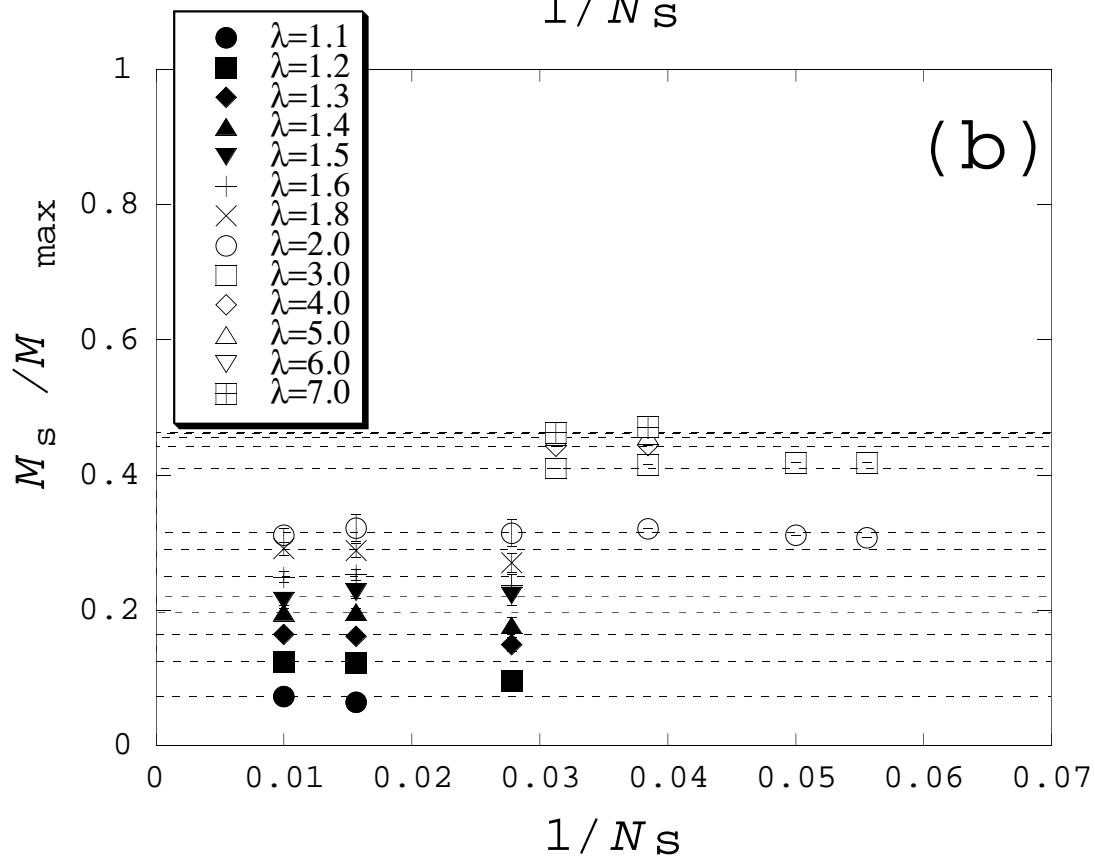
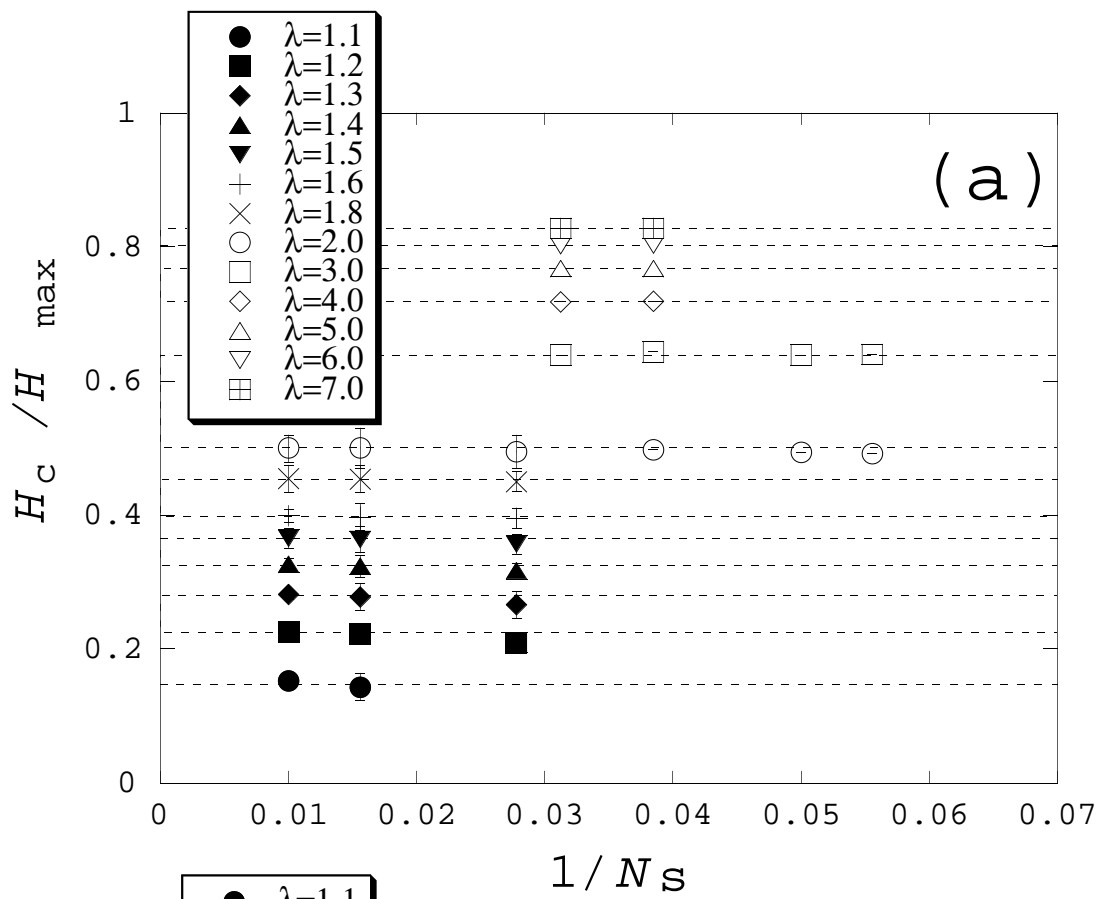


Fig.1(a)(b)

M.Kohno, et.al.

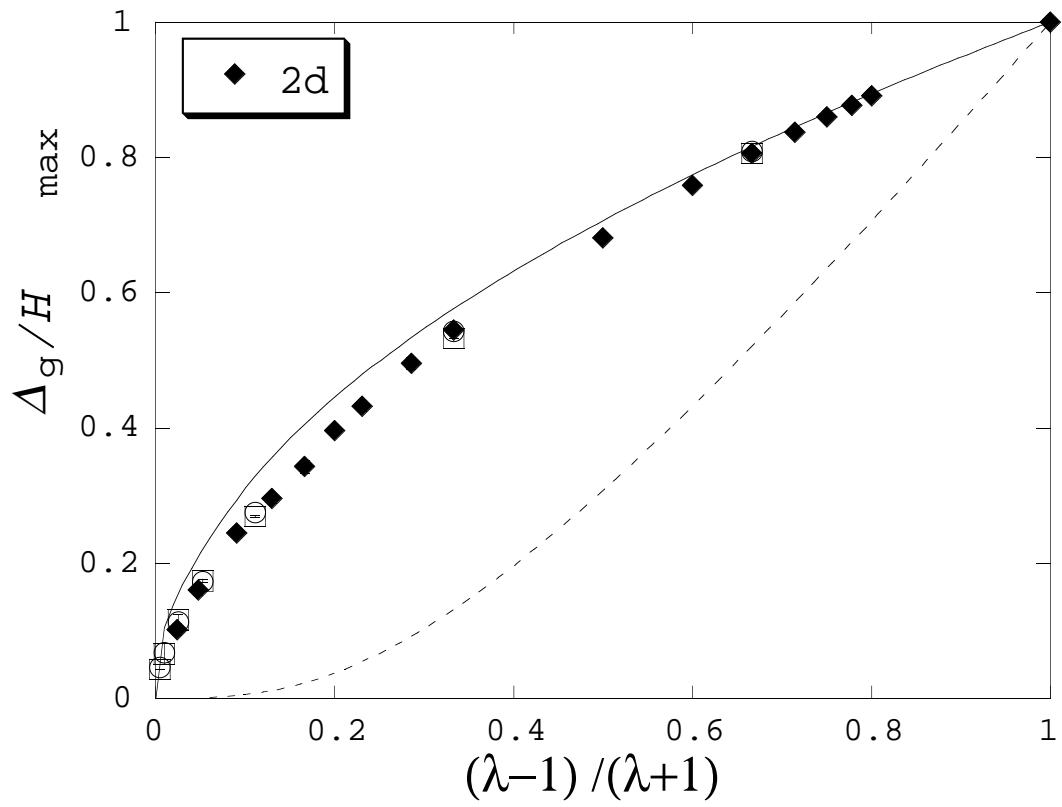
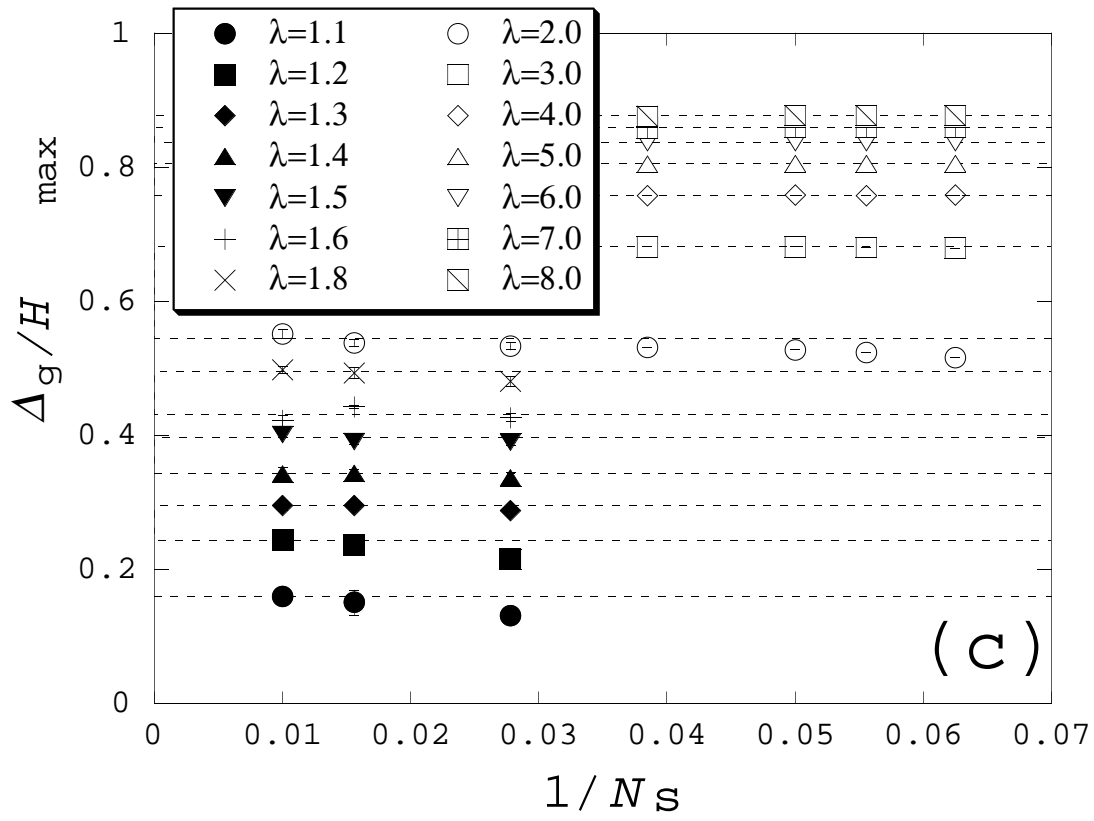


Fig.1(c), Fig2

M.Kohno, et.al.

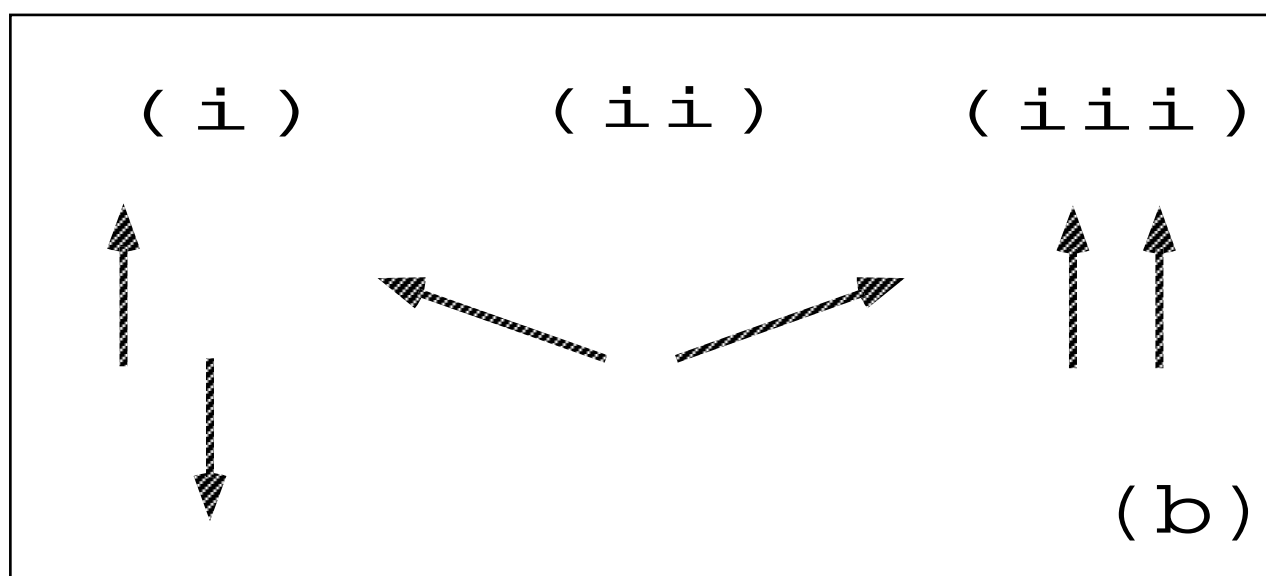
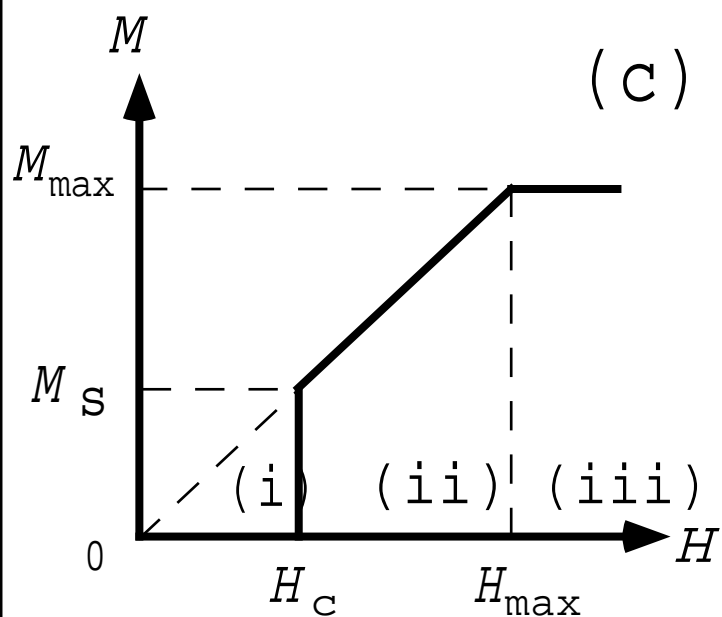
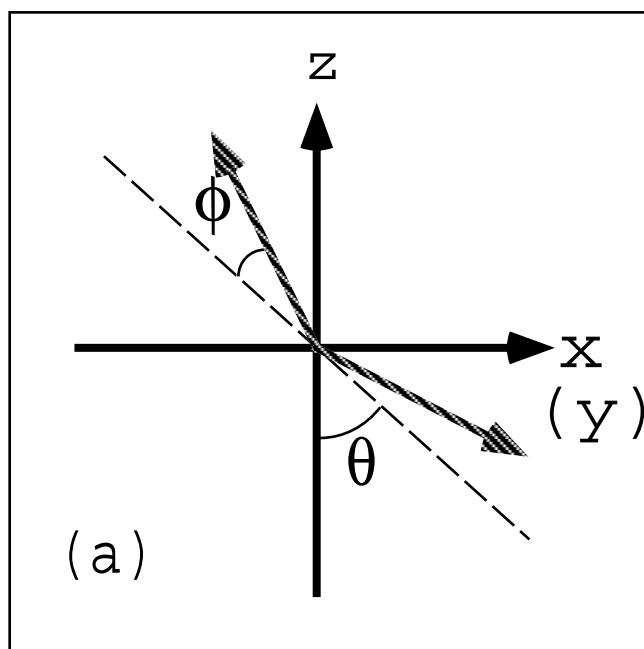


Fig.3(a), (b), (c) M.Kohno, et.al



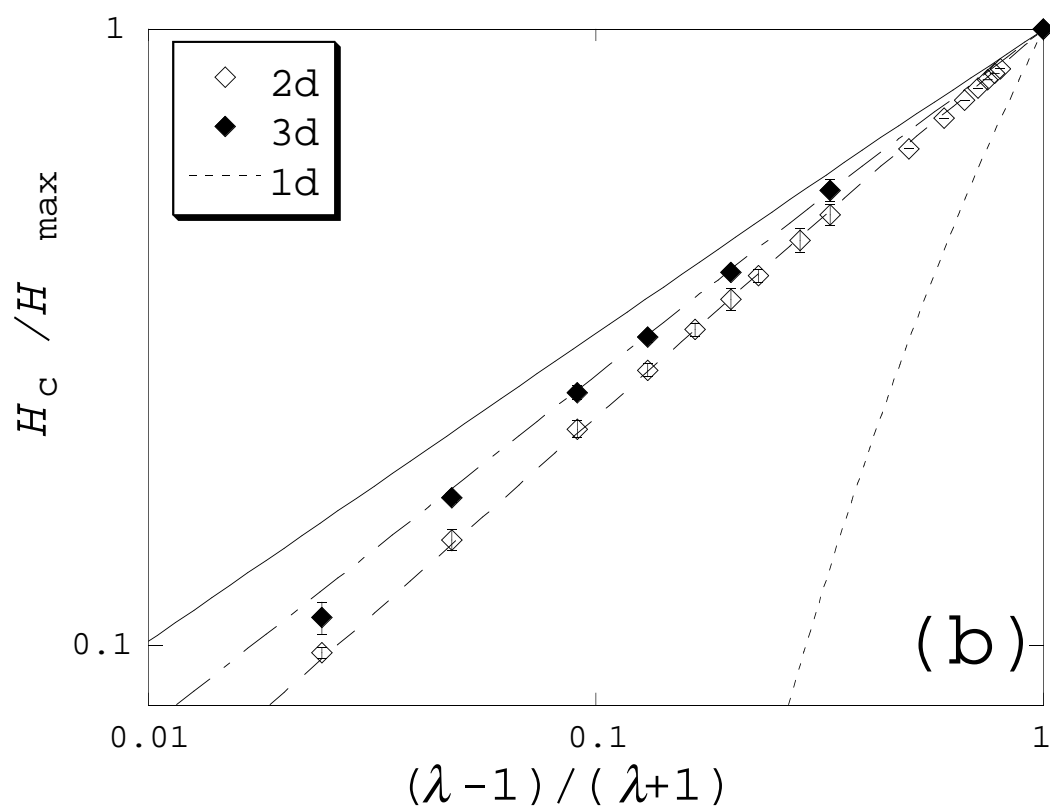
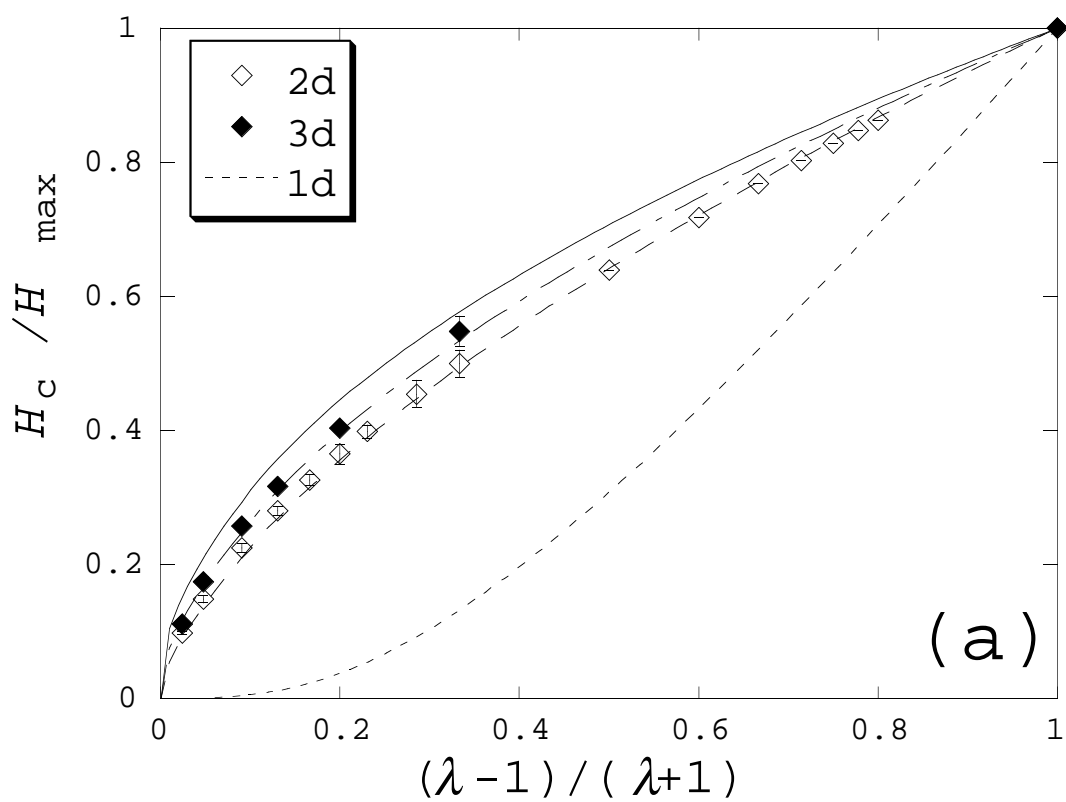


Fig.6(a)(b)

M.Kohno, et.al.

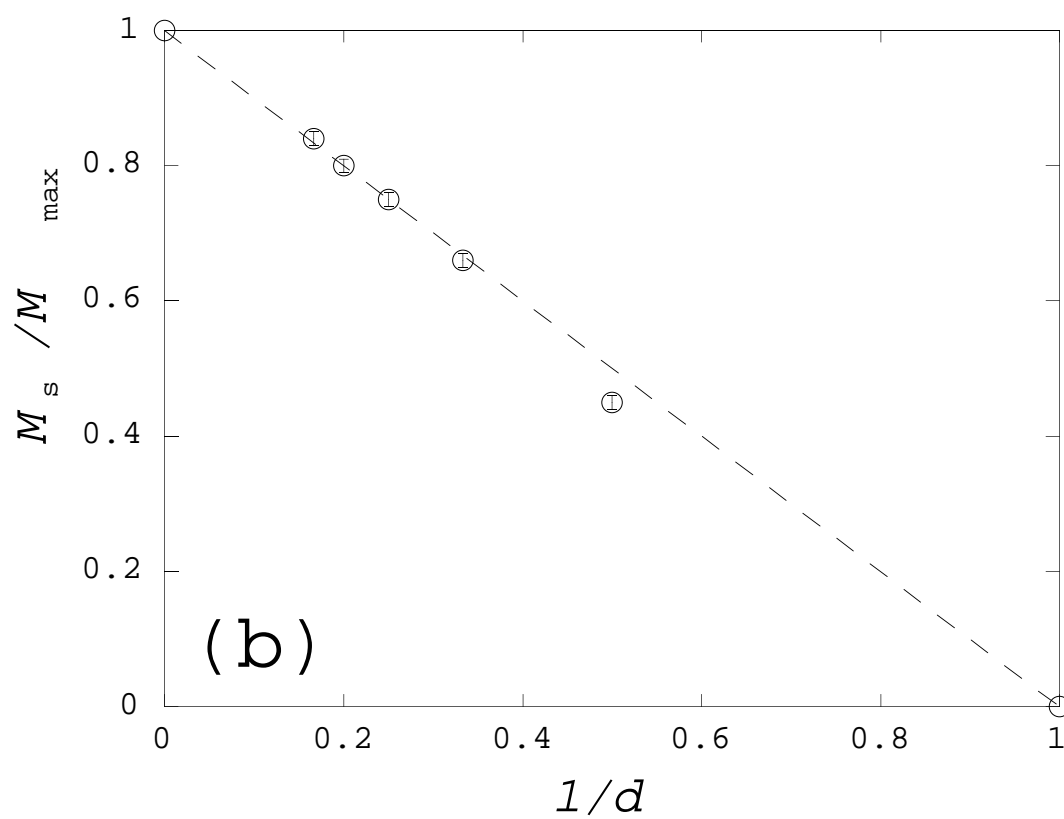
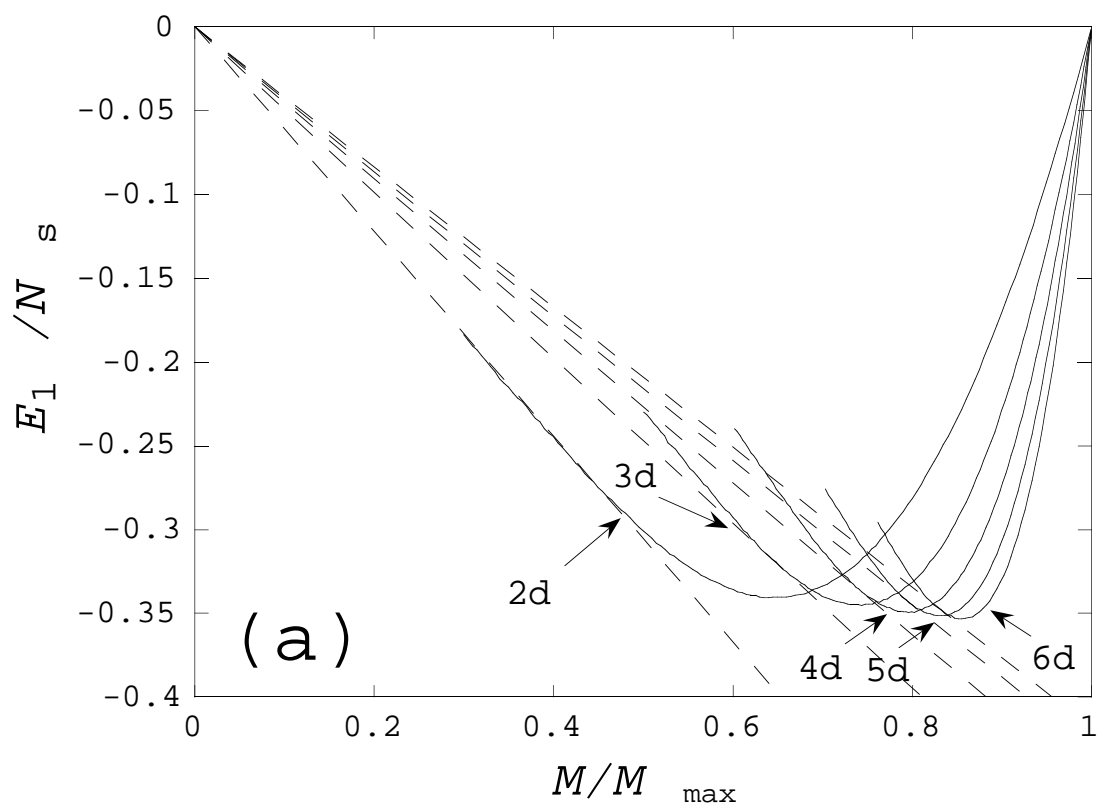


Fig.9(a)(b)

M.Kohno, et.al.

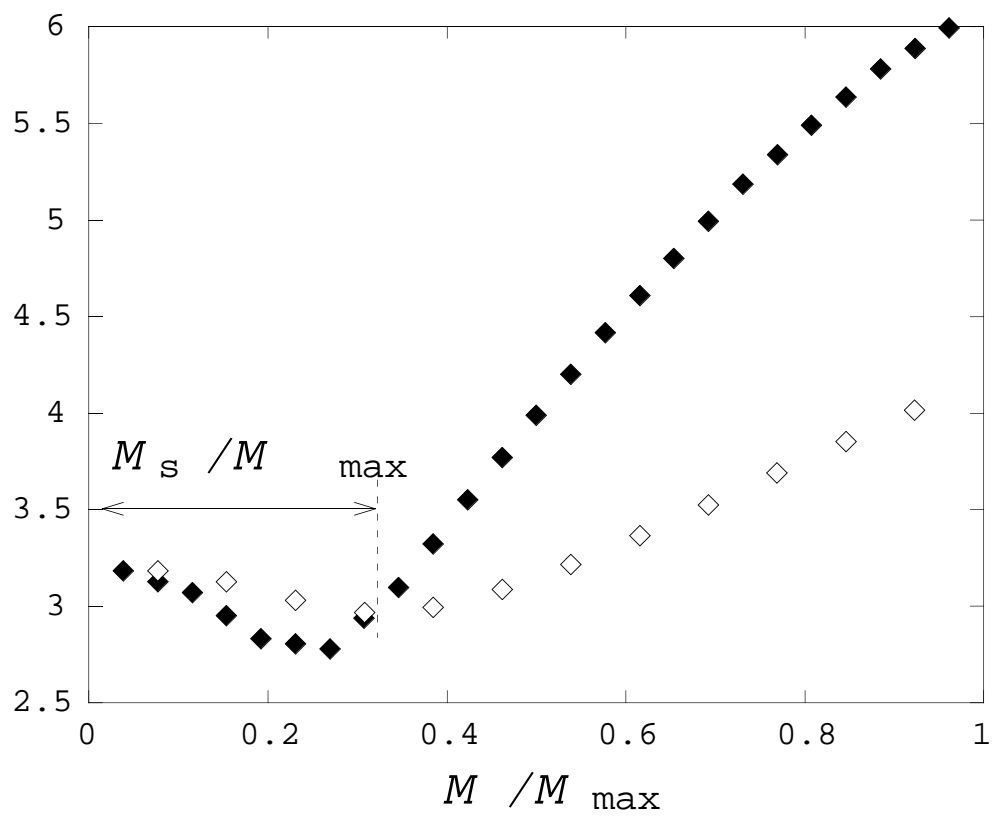
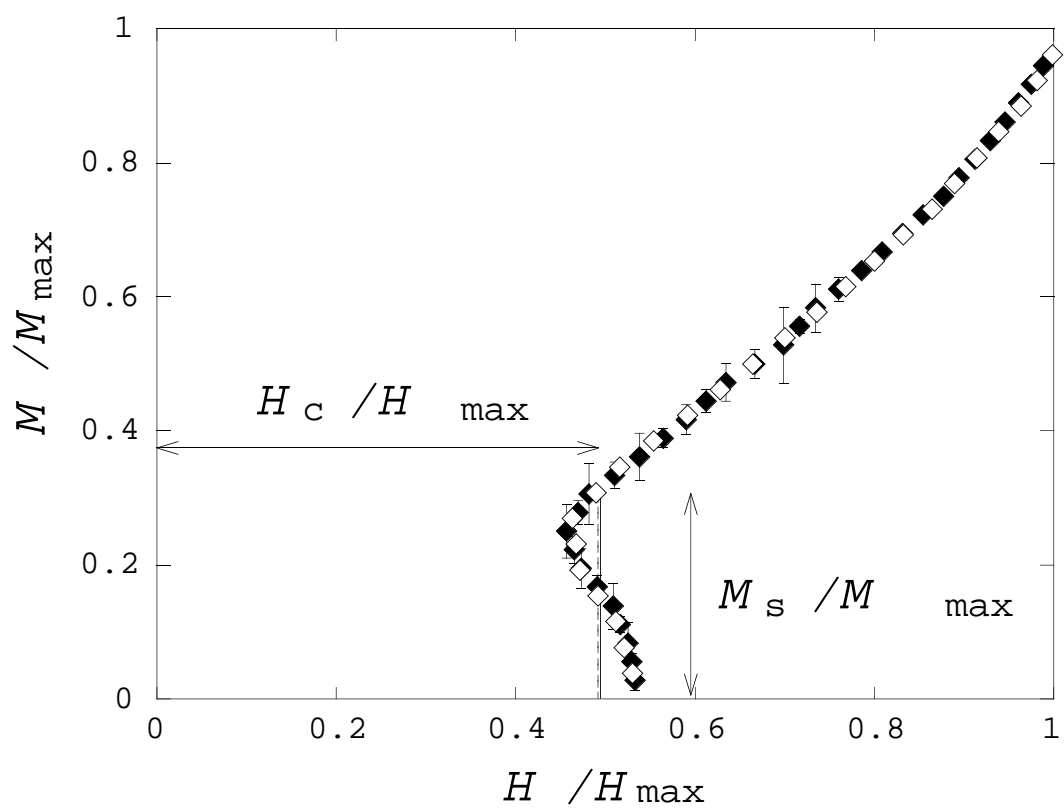


Fig.4,5 M.Kohno, et.al.

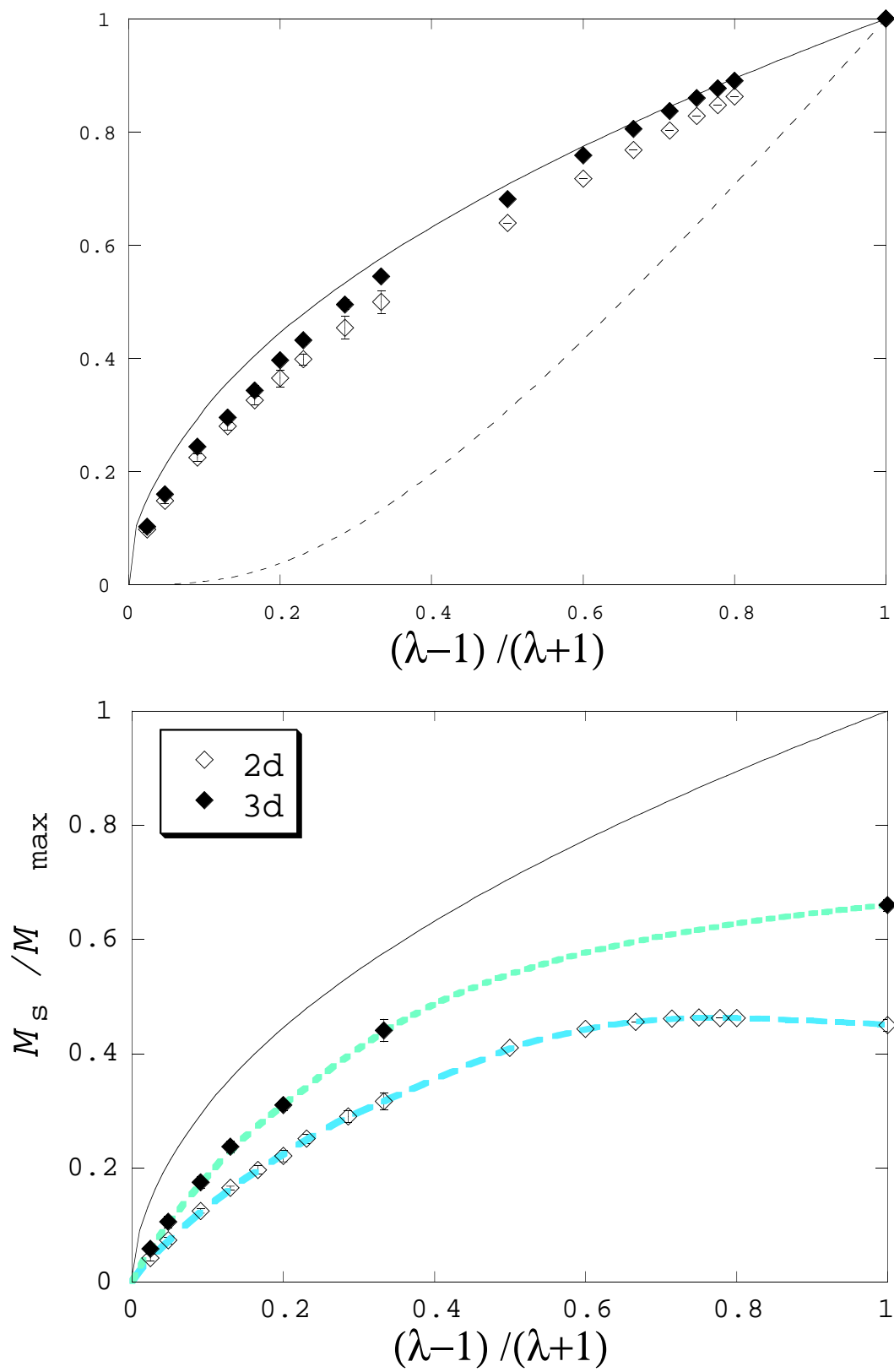


Fig.7,8

M.Kohno, et.al.